In phantom determination of collimator scatter factor

Kwok L. Lam and Randall K. Ten Haken
Department of Radiation Oncology, University of Michigan, Ann Arbor, Michigan 48109-0010

(Received 13 November 1995; accepted for publication 17 April 1996)

The collimator scatter factor S_c has generally been measured in air using an ionization chamber inside a buildup cap or mini-phantom. Here, S_c was measured in phantom at 10 cm depth for 6 and 15 MV photons with square collimator settings of 2.5–40.0 cm. The results were consistent with in air measurements with a mini-phantom to within 0.4%. In the measurements, a series of Cerrobend field shaping blocks were used to define the field size in the phantom while the collimator settings were varied from the field size in the phantom to twice that value. Corrections of up to 2% for scattered radiation from the added Cerrobend field shaping blocks were necessary. Since a buildup cap or mini-phantom is not used, the smallest field size that can be measured is limited only by the size of the detector and the measurement is performed with full scatter resembling the treatment condition of a patient.

I. INTRODUCTION

According to Khan,[1] the absorbed dose on the central axis can be written as

$$D_d = D_0(t_0, \mathrm{SSD}_0 + t_0) \times \left(\frac{\mathrm{SSD}_0 + t_0}{\mathrm{SSD} + d} \right)^2 S_c(r_c) S_p(r_d) \mathrm{TPR}(d, r_d). \quad (1)$$

The symbols follow those used in Ref. 1 and we have replaced TMR by the tissue phantom ratio, TPR. In this formalism, the relative output factor in phantom $S_{cp}(r_c; r_d)$ can then be expressed as

$$S_{cp}(r_c; r_d) = S_c(r_c) S_p(r_d). \quad (2)$$

The collimator scatter factor, S_c, of a high-energy photon beam is usually measured in air with a buildup cap[1] or mini-phantom.[2] However, when the collimator scatter factor for high-energy photon beam was introduced by Holt[3] *et al.*, it was extracted from in-phantom measurements taken at different distances and collimator settings. There are potential advantages to being able to determine S_c from measurements in a full scatter phantom instead of in air. First, the experimental conditions closely resembles the treatment conditions of a patient. Second, the smallest field size that can be measured is limited only by the size of the detector and not by the size of the buildup cap or mini-phantom (which is no longer present).

If $\mathrm{SSD} = \mathrm{SSD}_0$, $d = t_0$ and r_d is fixed while r_c is varied (that is, only S_c changes), it should be possible to extract $S_c(r_c)$ from measured D_d. However, one attempt to do this using a low melting point alloy field shaping block suggested[4] significant differences between $S_c(r_c)$ measured with this technique and $S_c(r_c)$ measured in air. In the course of making similar, though more extensive, measurements, we conjectured that differences between the in-air and in-phantom determination of S_c would arise (i) if scattered radiation from the treatment head, which contributed significantly[5–8] to the dependence of S_c on r_c, was partially shielded by the Cerrobend block when $r_c \gg r_d$; and (ii) if there was added scattered radiation from the Cerrobend block to the detector that was not included in Eq. (1). Here, we report on an in-phantom determination of $S_c(r_c)$ using measurement techniques and data reduction methods that take these factors into consideration.

II. METHODS AND MATERIALS

A. In-phantom measurements for determination of the collimator scatter factor

The in-phantom measurements were taken in a water phantom with the Wellhofer IC-10 chamber on a Varian Clinac 2100C equipped with a multileaf collimator (MLC). Data were taken with 6 and 15 MV x rays. The center of the chamber was at 100 cm from the target and at 10 cm depth along the central axis of the x-ray beam. This is the geometry used in our clinic for normalization of S_p's and TPRs [i.e., $\mathrm{SSD}_0 = 90$ cm and $t_0 = 10$ cm in Eq. (1)]. The experimental setup is shown in Fig. 1. Two sets of measurements were performed.

In the first set of measurements, a Cerrobend field shaping block (7.6 cm thick) defining a 5 cm×5 cm square irradiated field at the isocenter was used. The block was large enough to block the radiation outside of the 5 cm square field up to a 30 cm×30 cm collimator setting. Data were taken with collimator settings ranging from 5 cm×5 cm to 30 cm×30 cm. Uncorrected measured values of collimator scatter factor $\tilde{S}_c(r_c)$, where r_c was the collimator setting, were obtained by normalization of the measurements to the measurement at $r_c = 10$ cm. Additional data were taken with the MLC (mid-line 50.7 cm from the target) set to define an 8 cm×8 cm field at the isocenter together with the same 5 cm×5 cm Cerrobend block (the top of the block at 57.8 cm from the target). Similar to the analysis in Appendix A, it can be shown that the MLC will be behind the 5 cm×5 cm Cerrobend block from the point of view of the detector at the isocenter when the MLC is set to field sizes larger than 6.7 cm×6.7 cm. Thus, at a MLC setting of 8 cm×8 cm, the region of treatment head visible from the detector was *not* determined by the MLC and collimator scatter was not af-

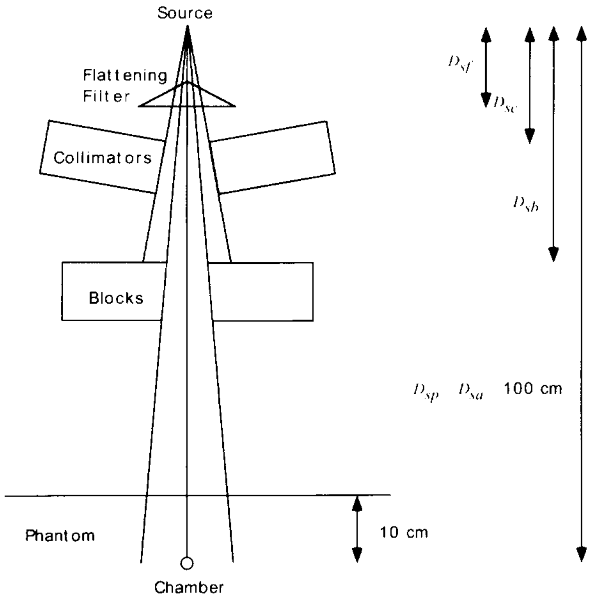

FIG. 1. Experimental setup, MLC located between collimators and blocks.

fected by the MLC. Moreover, the field size on the phantom r_d was defined by the Cerrobend block and phantom scatter was not affected by the MLC also. The MLC should have no effect on these measurements under these experimental conditions. This set of measurements was designed to test if corrections for effects not explicitly considered in Eq. (1) were necessary. The jaw settings were varied between 5 cm×5 cm and 25 cm×25 cm due to the limited size of the MLC on the Clinac 2100C. $\tilde{S}_c(r_c)$ were obtained by normalization of the measurements to the measurement with MLC and $r_c = 10$ cm.

In the second set of measurements, a series of secondary Cerrobend blocks (7.6 cm thick) was used. The focused blocks were made with square cross sections including square openings in the center. For a given block, r_d was determined by its opening, which projected to r_b at the isocenter from the source. Since the measurements were taken at the isocenter, r_d was equal to r_b. To ensure that scattered radiation from the treatment head reached the detector, we limited the collimator setting, r_c, used on a given block to αr_b, where α depended on the geometry of the treatment machine and the location of the detector (Appendix A). For a Clinac 2100C with a source to block tray distance of 65.4 cm, α was taken to be 2 when the chamber was at the isocenter. Thus, four blocks defining square field sizes r_b of 2.5, 5.0, 10.0, and 20.0 cm at the isocenter were sufficient. (The outer limits of each secondary block were also limited to 5.5, 10.5, 20.5, and 40.2 cm to reduce weight.) Measurements were taken with r_c of 2.5 to 5.0 cm, 5.0 to 10.0 cm, 10.0 to 20.0 cm, and 20.0 to 40.0 cm for r_b of 2.5, 5.0, 10.0, and 20.0 cm, respectively. Uncorrected measured values of the relative output factor in phantom $\tilde{S}_{cp}(r_c;r_d)$ were obtained by normalization of the measurements to the measurement of $r_c = r_d = 10$ cm. The measured $\tilde{S}_{cp}(r_c;r_d)$ will have discrete breaks at r_c of 5.0, 10.0, and 20.0 cm because r_d also changes at these r_c.

B. Scattered radiation from field shaping block

1. Scattered radiation emitted from lower surface of block

In order to measure the amount of scattered radiation from the lower surface of the Cerrobend block, transmissions through Cerrobend were measured with a block covering the whole area of the block tray (actually, three slabs of Cerrobend, each 2.5 cm thick for ease in handling). Measurements of ionization per MU at 10 cm depth with the chamber at the isocenter in a water phantom were taken with r_c varied from 2.5 to 40.0 cm and then normalized to that of a 10 cm by 10 cm open field. These normalized measurements of block transmission $T_b(r)$ represent the sum of scattered radiation and primary transmission. These measured $T_b(r)$ were fitted to a second-order polynomial using the linear-least-squares method. The block scatter from the lower surface of a block is then estimated to be

$$S_b(r_c;r_b) = T_b(r_c) - T_b(r_b). \quad (3)$$

2. Scattered radiation emitted from side surface of block

We estimated the amount of scattered radiation emitted from the inside surface of the opening of the Cerrobend block to the isocenter based on the analytical first scatter model of Ahnesjö.[9] Here we took into account the scattered radiation that comes from radiation incident on the top of the Cerrobend block but neglected scattered radiation that comes from radiation incident on the side of the block. We designated the side scatter factor $S_s(r_c;r_b)$ to be the energy fluence of scattered radiation to the isocenter from the side of the block, normalized to the energy fluence at the isocenter. It can be shown (Appendix B) that $S_s(r_c;r_b)$ can be approximated as

$$S_s(r_c;r_b) = \kappa r_b\{1 - \exp[-\beta\mu_s(r_c - r_b)]\}, \quad (4)$$

where κ is the scatter per unit field size, β is the scaling from field sizes to pathlength in the block, and μ_s is the attenuation coefficient of Cerrobend. Numerical values used in the estimate are shown in Appendix B.

C. Determination of collimator scatter factor

The total relative output factor $S_{cp}(r_c;r_d)$ after correction for scattered radiation from the block is (note $r_d = r_b$ in the measurements)

$$S_{cp}(r_c;r_d) = \tilde{S}_{cp}(r_c;r_d) - S_b(r_c;r_b) - S_s(r_c;r_b). \quad (5)$$

At the breakpoints in the measurements, when, for example, a Cerrobend block of field size $r_b = r_c/2$ is replaced by one of field size $r_b = r_c$ at the collimator setting r_c, we have $S_{cp}(r_c;r_c/2)$ and $S_{cp}(r_c;r_c)$. These values differ only by the ratio of S_p's:

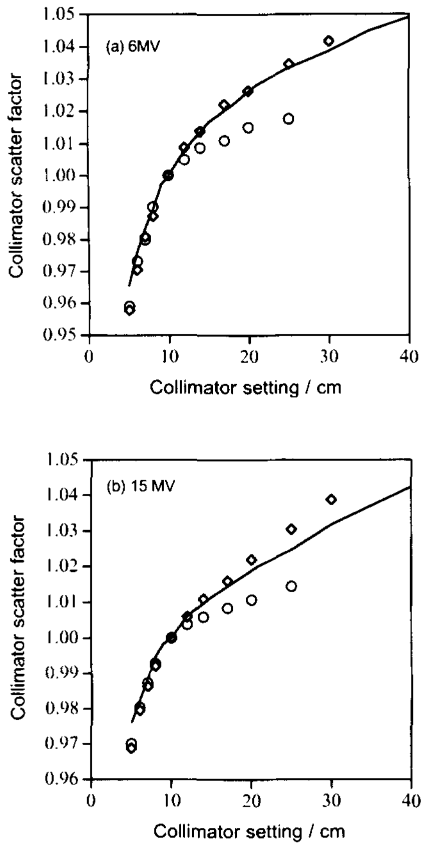

FIG. 2. Comparison of collimator scatter factor measured in air and collimator scatter factors obtained by using a 5 cm×5 cm Cerrobend block. Solid lines are collimator scatter factors measured in air. Diamonds are collimator scatter factors measured with only a 5 cm×5 cm Cerrobend block opening. Circles are collimator scatter factors measured with a 5 cm×5 cm Cerrobend block opening and an 8 cm×8 cm opening formed by the MLC. (a) 6 MV. (b) 15 MV.

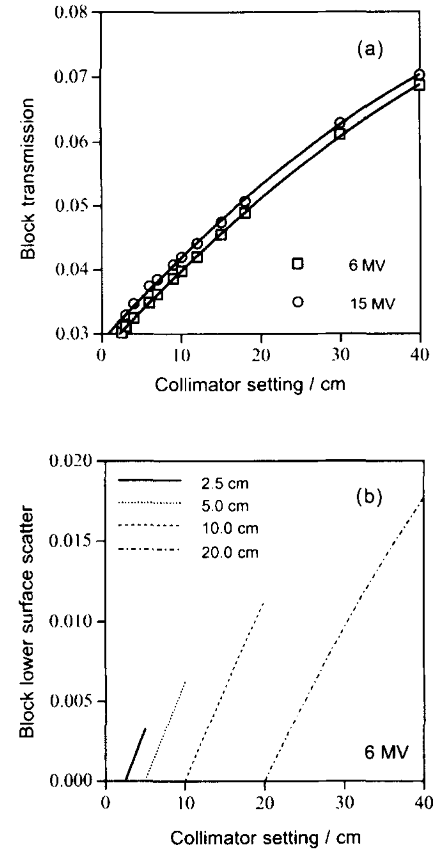

FIG. 3. (a) Transmission through the Cerrobend block at 10 cm depth normalized to dose at the isocenter for a 10 cm square open field. The solid lines are second-order polynomial fits to the data. (b) Scatter from the Cerrobend blocks for 6 MV computed from the polynomial fit shown in (a). Sizes indicated in the legend are openings of blocks projected to the isocenter. Results for 15 MV are within 0.0005 of that for 6 MV.

$$\frac{S_p(r_c)}{S_p(r_c/2)} = \frac{S_{cp}(r_c;r_c)}{S_{cp}(r_c;r_c/2)}. \tag{6}$$

Thus $S_p(5.0)/S_p(2.5)$, $S_p(10.0)/S_p(5.0)$, and $S_p(20.0)/S_p(10.0)$ were determined. As $S_p(10.0)$ was defined to be 1.0, the other S_p's were computed from the ratios. S_c was then determined from Eq. (2) with the corrected $S_{cp}(r_c;r_d)$ and the derived $S_p(r_d)$. That is,

$$S_c(r_c) = S_{cp}(r_c;r_d)/S_p(r_d). \tag{7}$$

Since only four different values of r_d were used in the measurement of $\tilde{S}_{cp}(r_c;r_d)$, the four S_p's determined from Eq. (6) above were sufficient to determine $S_c(r_c)$ from Eq. (7) for all r_c's used in the experiment (between 2.5 and 40 cm).

III. RESULTS

In Fig. 2, $\tilde{S}_c(r_c)$ measured with a 5 cm×5 cm blocked field, without and with MLC defining an 8 cm×8 cm opening for different collimator settings are compared with in-air measurements of S_c on the same treatment unit using a miniphantom at 10 cm depth. Details of the in-air measurements were reported elsewhere.[10]

In Fig. 3(a), block transmissions $T_b(r)$ through a 7.6 cm thick Cerrobend block for both 6 and 15 MV are shown. The transmissions were fitted to a second-order polynomial to reduce the effect of random error and to interpolate between measured values. The block scatter S_b deduced from T_b [Eq. (3)] for 6 MV are shown in Fig. 3(b). The difference between S_b's of 6 and 15 MV are less than 0.0005.

Figure 4 illustrates the analytical result of the side scatter factor $S_s(r_c;r_b)$ for blocks of field sizes 2.5, 5.0, 10.0, and 20.0 cm. Since only radiation entering the block from the top and scattered to the side was considered, the graphs start from zero when the collimator setting is the same as the field size of the block. S_s approaches 0.005 for the 20.0 cm block. S_s can also be considered to be independent of energy for the beam qualities used.

In Fig. 5, the measured $\tilde{S}_{cp}(r_c;r_d)$ are compared with the corrected [Eq. (5)] $S_{cp}(r_c;r_d)$. The scatter correction is over 2% for $r_c = 40$ cm. The breaks at 5.0, 10.0, and 20.0 cm are due to changes in field shaping blocks.

The S_c obtained from in phantom measurements [Eq. (7)] are compared with values obtained from in-air measurements[10] in Fig. 6. Results from the two techniques are within 0.4%.

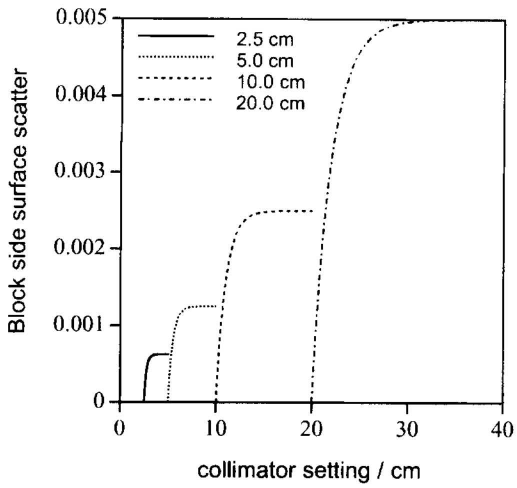

FIG. 4. Scatter radiation energy fluence from the side of the opening of the Cerrobend block normalized to incident energy fluence at the isocenter. The legend indicates the field size at the isocenter defined by the opening.

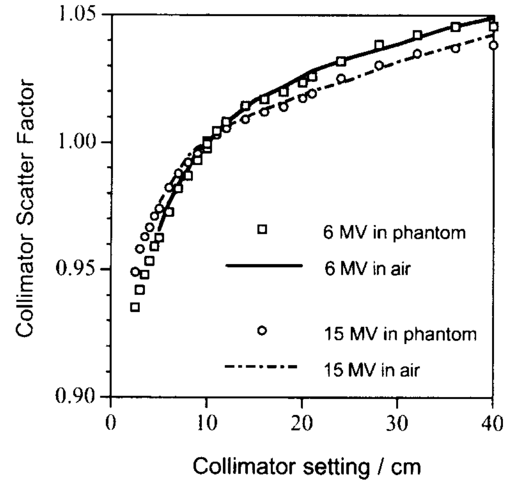

FIG. 6. Comparison of collimator scatter factors measured in phantom and in air.

IV. DISCUSSION

The uncorrected $\tilde{S}_c(r_c)$ (Fig. 2) measured in phantom with and without MLC are inconsistent with each other and are inconsistent with in-air measurements, especially for 15 MV. According to the formalism of Eq. (1), the MLC should have no effect on these measurements under these experimental conditions (see Sec. II A). The difference between the data points with and without the MLC (circles and diamonds in Fig. 2, respectively) is a direct demonstration that a measurable effect on dose is not accounted for in Eq. (1) under some specific conditions. We interpret the difference between the measurements with and without the MLC to be the loss of scattered radiation from the Cerrobend block when the MLC partially shields the Cerrobend block from primary radiation for collimator settings larger than 8 cm×8 cm.

Also in Fig. 2, with the MLC shielding the extra scattered radiation for a collimator setting larger than 8 cm×8 cm, the measured $\tilde{S}_c(r_c)$ increases much less than the in-air S_c with increasing collimator settings beyond 12 cm×12 cm. We attribute[10] this difference to the 5 cm×5 cm Cerrobend block limiting the view of scattered radiation in the area of the flattening filter from the detector; a second effect that can directly affect the S_c part of Eq. (1). According to the estimate in Appendix A, the 5 cm×5 cm projected opening Cerrobend block (and hence not the collimator) limits the view of the flattening filter in the direction of the lower jaws when the setting of the lower jaws is more than 11.5 cm.

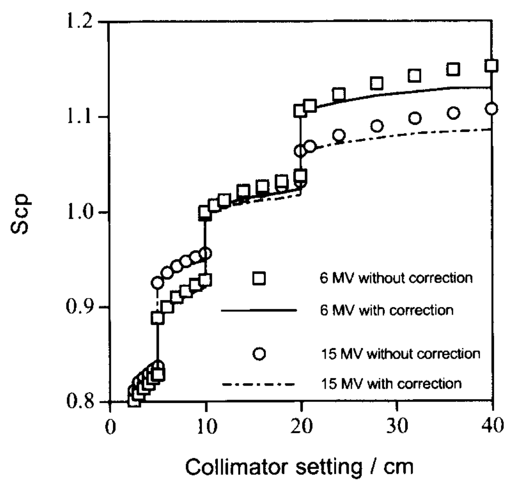

FIG. 5. Comparison of S_{cp} with and without correction for scatter from the Cerrobend block.

From Fig. 3(a), the scattered radiation at isocenter attributed to block scatter at 10 cm deep in a water phantom from a 40 cm Cerrobend block is over 3% of a 10 cm square open field. Thus, this can be a significant correction if Cerrobend blocks are used for the in-phantom determination of S_c. The corrections for scattered radiation used here are applicable to scattered photons. Electron contamination from the field shaping block was not considered. Since the measurements were performed at a depth of 10 cm, electron contamination was not important. If measurements were taken at a depth of maximum dose, corrections for electron contamination from the side and lower surfaces of the block would need to be determined. Beyond the determination of S_c, further studies are needed to evaluate the clinical importance of correction for scatter from the lower surface of field shaping blocks for heavily blocked treatment fields, such as mantle fields.

The normalized scattered radiation from Cerrobend differs by less than 0.0005 between 6 and 15 MV. Due to this insensitivity to energy and the correction being of the order of only a few percent, the normalized scattered radiation can potentially be quantified as a function of beam quality with sufficient accuracy for commonly used materials. Measurements specific to a particular treatment machine can then be avoided.

On the Varian Clinac 2100C, the MLC together with the Cerrobend block potentially have enough thickness so that the correction for scattered radiation from field shaping devices may not be necessary. Currently, the MLC on Clinac

2100C is limited to a maximum field size of 26 cm×26 cm. Further studies are needed to investigate the possibility of measuring S_c in phantom without block scatter correction if a MLC of larger field size is available.

From Fig. 4, the scattered radiation from the side surface of the block, $S_s(r_c;r_b)$, is a small correction (less than 0.5% in our experiment). Thus, accurate determination of $S_s(r_c;r_b)$ for each specific machine is not necessary.

The consistency between in-air and in-phantom measurements shown in Fig. 6 demonstrates that S_c can be extracted from in-phantom measurements when scatter from the Cerrobend block and the view of the flattening filter are taken into account in the design and analysis of the measurements. In practice, the following steps need to be followed to measure S_c. The lower limit and upper limit of field sizes $r_{\min}$ and $r_{\max}$, respectively, for the determination of S_c are decided and α in Eq. (A1) is computed. $N+1$ Cerrobend blocks with r_b's (block field sizes) equal to $r_{\min}$, $\alpha r_{\min}$, $\alpha^2 r_{\min},\ldots,\alpha^N r_{\min}$, where $r_{\max}/\alpha<\alpha^N r_{\min}<r_{\max}$, are made. Measurements of $\tilde{S}_{cp}$ are then made at the isocenter with the $N+1$ blocks using collimator settings between and including the field sizes r_b and αr_b for each block, and the $\tilde{S}_{cp}$ are normalized. Transmission T_b of a solid Cerrobend block at all field sizes used are also measured and normalized. S_b's are calculated from Eq. (3). S_s's are calculated from Eq. (4) using numerical values in Appendix B. S_{cp}'s are calculated from Eq. (5). S_c's are obtained from Eq. (7) using S_p's from Eq. (6).

The smallest field size used in the measurement was 2.5 cm and the Wellhofer IC-10 chamber has an inside diameter of 0.6 cm. Although we have not investigated the effect of chamber size on measurements with small fields, chambers with a smaller diameter can be used if more accurate measurements or smaller field sizes are desired.

V. CONCLUSION

We have shown that by use of a series of field shaping blocks to define the field in the phantom so that the region of treatment head visible from the measurement point is defined by the adjustable collimator, S_c can be accurately determined from measurements in phantom when scattered radiation from the field shaping block is corrected for. Thus, S_c may be determined under circumstances more closely related to the situation under which patients are treated and for field sizes limited only by the detector size.

APPENDIX A: RANGE OF COLLIMATOR SETTING FOR A GIVEN FIELD SIZE

The purpose of limiting the range of collimator settings is to ensure that the region of the treatment head at the level of the flattening filter visible from the point of view of the chamber is defined by the collimator. Head scatter is assumed to come primarily from the level of the flattening filter.[10] Let (Fig. 1) the source to axis distance be D_{sa}, source to flattening filter distance be D_{sf}, the source to top of collimator distance be D_{sc}, the source to top of block distance be D_{sb}, and the source to measurement point distance be D_{sp}. Then the physical dimension of the opening of the collimator for a collimator setting of r_c is $r_c(D_{sc}/D_{sa})$ and the projection of this dimension to the level of the flattening filter from the measurement point is $r_c(D_{sc}/D_{sd})[D_{sp}-D_{sf}/D_{sp}-D_{sc}]$. Similarly, the projection of the opening of the block to the level of the flattening filter is $r_b(D_{sb}/D_{sa})[D_{sp}-D_{sf})/D_{sp}-D_{sb}]$. When these two expressions are equal, r_c is at the maximum opening that the region projected from the collimator is not clipped by that from the block. The solution gives the maximum collimator setting as

$$r_b\,\frac{D_{sb}D_{sp}-D_{sc}}{D_{sc}D_{sp}-D_{sb}};$$

i.e.,

$$\alpha=\frac{D_{sb}}{D_{sc}}\,\frac{D_{sp}-D_{sc}}{D_{sp}-D_{sb}}. \tag{A1}$$

The minimum collimator setting that will not clip the field defined by the block in the phantom is r_b. In summary, r_c can be adjusted between r_b and αr_b to vary the scatter from the treatment head without affecting the field size on the phantom.

For the Varian Clinac 2100C with source to tray distance of 65.4 cm, and block thickness of 7.6 cm, D_{sb} is 57.8 cm. Since D_{sp} is 100.0 cm for the measurements, α is 3.6 for the upper jaws, which has a D_{sc} of 27.6 cm. For the lower jaws, D_{sc} is 37.0 and α is 2.3. We have limited the range of r_c to be r_b to $2r_b$ in the measurements so that neither the region defined by the upper jaws nor that defined by the lower jaws is clipped.

APPENDIX B: SCATTERED RADIATION FROM THE SIDE SURFACE OF THE BLOCK

Ahnesjö demonstrated that the majority of the scattered radiation from a block was first scattered radiation.[9] The geometry of the interactions is shown in Fig. 7. We have approximated the pathlength l of the scattered photon in the block to be proportional to the distance, x, of the point of entry from the block edge for the primary radiation, i.e., $l=Bx$. Following Ahnesjö, we express the energy fluence Ψ at the point of measurement as the integral of the contributions from first scattered radiation over the volume of the block. However, instead of integrating over $x\in[0,\infty]$ as done in Ref. 9, we integrate over

$x\in[0,X]$:

$$\begin{aligned}\Psi&=\int_0^X \psi\exp(-\mu_s Bx)\,dx\\&=\frac{\psi}{\mu_s B}[1-\exp(-\mu_s BX)]=\Psi_c[1-\exp(-\mu_s BX)],\end{aligned} \tag{B1}$$

where X is the width of the block that is irradiated and μ_s is the attenuation coefficient of the scattered radiation. ψ is a measure of the amount of first scattered radiation generated as the primary radiation is attenuated in the block. If there is no attenuation for the scattered radiation (i.e., $\mu_s=0$),

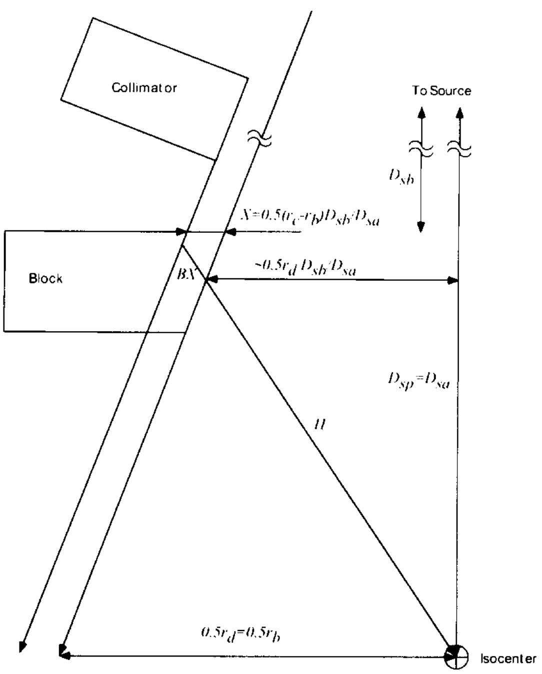

FIG. 7. Geometry for the pathlength in the Cerrobend block of scattered radiation emitted from the side surface.

$\psi = d\Psi/dX$ from the first equality in Eq. (B1). Thus ψ is the scattered radiation energy fluence per unit width of block at the point of measurement if there is no attenuation for the scattered radiation in the block. The dependence of ψ on x due to inverse-square law is small compared with the variation of $\exp(-\mu_s Bx)$ so that ψ can be considered to be independent of x in the integral. Note that as $X\rightarrow\infty$, $\Psi\rightarrow\Psi_c$. Thus Ψ_c is the inner edge component (i.e., when the alignment angle α in Ref. 9 is set to zero) of collimator scatter in Ref. 9. In Fig. 7, using similar triangles, we have

$$BX = X\left(\frac{H}{0.5r_d}\right) = 0.5(r_c - r_b)\,\frac{D_{sb}}{D_{sa}}\left(\frac{H}{0.5r_d}\right)$$

$$\cong (r_c - r_b)\,\frac{D_{sb}}{D_{sa}}\,\frac{D_{sp}-D_{sb}}{r_d}. \tag{B2}$$

If we normalize the energy fluence in Eq. (B1) to the energy fluence Ψ_0 of a 10 cm square field size and substitute BX from Eq. (B2), Eq. (B1) can be written as

$$\frac{\Psi}{\Psi_0} = \frac{\Psi_c}{\Psi_0}\left[1-\exp\left(-\mu_s(r_c-r_b)\,\frac{D_{sb}}{D_{sa}}\,\frac{D_{sp}-D_{sb}}{r_d}\right)\right]. \tag{B3}$$

In Fig. 8 of Ref. 9, the energy fluence of the scattered radiation of a 40 cm square field is 0.49% of the energy fluence of the open field at 10 MV for zero degree alignment angle and the corresponding values are 0.63% and 0.26% at 4 and 24 MV, respectively. If we take into account the two times difference in the amount of scatter radiation between Cerrobend and tungsten (Table III in Ref. 9), for a 40 cm square field, Ψ_c/Ψ_0's are 1.3%, 0.98%, and 0.52% at 4, 10, and 24 MV, respectively. This dependence on energy of Ψ_c/Ψ_0 for a 40 cm square field can be well approximated by $\Psi_c/\Psi_0 = 0.014 - 0.000\,34E(\mathrm{MV})$, where $E(\mathrm{MV})$ is the accelerating potential[9] in MV. Based on Fig. 5 in Ref. 9, Ψ_c/Ψ_0 is approximately proportional to the opening r_b of the block. We can write, $\Psi_c/\Psi_0 = \kappa r_b$ and

$$\frac{\Psi}{\Psi_0} = \kappa r_b\left[1-\exp\left(-\mu_s(r_c-r_b)\,\frac{D_{sb}}{D_{sa}}\,\frac{D_{sp}-D_{sb}}{r_d}\right)\right], \tag{B4}$$

where

$$\kappa(\mathrm{cm}^{-1}) = 3.4\times10^{-4} - 8.6\times10^{-6}E(\mathrm{MV}). \tag{B5}$$

By comparing Eq. (4) and Eq. (B4),

$$\beta \cong \frac{D_{sb}}{D_{sa}}\,\frac{D_{sp}-D_{sb}}{r_b}. \tag{B6}$$

Since κ varies insignificantly between 6 and 15 MV, we have used 0.000 25 cm^{-1} at 10 MV as κ for both 6 and 15 MV. Also, μ_s varies slowly between 1.5 and 20 MeV.[11] We have used μ_s of each element in Cerrobend at 2 MeV to obtain an effective μ_s of 0.416 cm^{-1} for both 6 and 15 MV.

[1]F. M. Khan, W. Sewchand, J. Lee, and J. F. Williamson, "Revision of tissue-maximum ratio and scatter-maximum ratio concepts for cobalt-60 and higher energy x-ray beams," Med. Phys. **7**, 230–237 (1980).

[2]J. J. M. van Gasteren, S. Heukelom, H. J. van Kleffens, R. van der Laarse, J. L. M. Venselaar, and C. F. Westermann, "The determination of phantom and collimator scatter components of the output of megavoltage photon beams: Measurement of the collimator scatter part with a beam-coaxial narrow cylindrical phantom," Radiother. Oncol. **20**, 250–257 (1991).

[3]J. G. Holt, J. S. Laughlin, and J. P. Moroney, "The extension of the concept of tissue-air-ratios (TAR) to high-energy x-ray beams," Radiology **96**, 437–446 (1970).

[4]P. D. Higgins, E. Lee, and A. Ahuja, "In-phantom measurement of collimator scatter factors," Med. Phys. **21**, 924 (1994) (abstract).

[5]K. R. Kase and G. K. Svensson, "Head scatter data for several linear accelerators (4–18 MV)," Med. Phys. **13**, 530–532 (1986).

[6]R. Mohan, C. Chui, and L. Lidofsky, "Energy and angular distribution of photons from medical linear accelerators," Med. Phys. **12**, 592–597 (1985).

[7]G. Luxton and M. A. Astrahan, "Output factor constituents of a high-energy photon beam," Med. Phys. **15**, 88–91 (1988).

[8]E. L. Chaney and T. J. Cullip, "A Monte Carlo study of accelerator head scatter," Med. Phys. **21**, 1383–1390 (1994).

[9]A. Ahnesjö, "Collimator scatter in photon therapy beams," Med. Phys. **22**, 267–278 (1995).

[10]K. L. Lam, M. S. Muthuswamy, and R. K. Ten Haken, "Flattening filter based empirical methods to parameterize the head scatter factor," Med. Phys. **23**, 343–352 (1996).

[11]E. Storm and H. I. Israel, "Photon cross sections from 1 keV to 100 MeV for elements $Z=1$ to $Z=100$," Nucl. Data Tables A **7**, 565–681 (1970).